23

Two-photon Imaging of Neocortical Microcirculation

DAVID KLEINFELD AND WINFRIED DENK

INTRODUCTION

Brain homeostasis depends on adequate levels of blood flow to ensure the delivery of nutrients and to facilitate the removal of catabolic products. The exchange of material between constituents in the blood and neurons and glia occurs at the level of individual capillaries, vessels that are 5–8 μm in caliber. An increase in the electrical activity within populations of neurons may subsequently result in increases and decreases of blood flow in activated and quiescent regions, respectively (Woolsey et al. 1996). These redistributions of blood flow, together with changes in the blood oxygenation levels, form the basis of functional MRI (Ogawa et al. 1990) and intrinsic optical imaging (Blasdel and Salama 1986; Grinvald et al. 1986; see also Chapters 45–47). Although these functional imaging methods are useful for mapping neural activity, their spatial resolution of 100 μm to 1 mm is too poor to study the microscopic mechanisms behind the control of cortical hemodynamics. However, cortical blood flow at the level of individual capillaries can be observed with high-resolution imaging techniques (Villringer et al. 1989; Dirnagl et al. 1992).

Here we review the methodological advantages and some technical aspects associated with the use of two-photon laser scanning microscopy (Denk et al. 1990), as opposed to confocal laser scanning microscopy (Villringer et al. 1989; Dirnagl et al. 1992), to image blood flow in neocortical microvasculature. Confocal laser scanning microscopy, in conjunction with fluorescent labeling of the blood plasma, can be used to observe the motion of individual red blood cells in single capillaries as dark objects against a bright background. However, the depth for which functional images are obtained is limited to approximately 150 μm below the pia mater with confocal laser scanning microscopy. In contrast, with two-photon microscopy we could obtain images down to 600 μm below the pia (Kleinfeld et al. 1998). Such a depth is sufficient to reach the middle layers of rat neocortex, where the density of synaptic terminals (Woolsey and Van Der Loos 1970), and hence activity-dependent energy consump-

tion, are greatest. These layers are also where the earliest electrical activity following a sensory stimulus is observed (Armstrong-James et al. 1992). The increased depth penetration of two-photon microscopy over confocal microscopy, which uses single-photon excitation, is the result of reduced scattering of near-IR as compared to visible light and the ability to collect emitted light even after it has been scattered by brain tissue (Denk et al. 1994, 1995; see also Chapter 17).

CHOICE OF ANIMAL

There is a considerable literature on the nature of cortical blood flow in rodents, predominantly rats and mice (Woolsey et al. 1996; Hudetz 1997). The most common species used in previous studies have been Wistar or Sprague-Dawley rats and Swiss-Webster mice. Rats are generally considered easier to maintain under prolonged periods of anesthesia and were used in our initial study (Kleinfeld et al. 1998). However, mice have a thinner cortex, i.e., approximately 1.6 mm total thickness versus 2.2 mm for rat, and many transgenic animals with various physiological mutations or functional markers are available in increasing variety (Johns et al. 1996; Merrill et al. 1997). The experimental procedures are described here for rats but should be readily adaptable to mice.

CHOICE OF ANESTHETIC

Whole-animal imaging experiments usually require the use of an anesthetic to immobilize the animal in a calm and pain-free state. However, anesthetics by their nature have a strong effect on the activity in the nervous system (see, e.g., Chapin et al. 1981; West 1998) and, thus, on the hemodynamics that is coupled to neural activity. The effects of the anesthetic used have to be taken into account specifically for each scientific question that is to be answered.

A brief compendium of anesthetics and dosages found in the rodent blood-flow literature is presented in Table 23.1. A more exhaustive review of anesthetics and their effects can be found in Flecknell (1987) and Short (1987).

We have used the widely popular agent, urethane. Like the related compound cloralose (the α-isomer), urethane produces a relatively stable basal blood flow, as measured via laser-Doppler flowmetry (Lindauer et al. 1993), and reproducible electrophysiological responses (Armstrong-James et al. 1992). However, both of these compounds are unsuitable when recovery from anesthetic is required. Halothane, which is gaseous and allows a rapid adjustment of the depth of anesthesia, can be used in those cases. Halothane, however, induces large spontaneous fluctuations in blood flow (Muldoon et al. 1988; Lindauer et al. 1993), as may isoflurane (Golanov et al. 1994).

Table 23.1. *Typical anesthetics and doses used in studies of cerebral blood flow in rat*

Agent (delivered i.p.)	Dose[a] (per kg rat)		Representative reference
	initial	supplement	
α-Chloralose	50 mg	40 mg/hr	Lindauer et al. (1993)
Ketamine plus	100 mg	30 mg	Wei et al. (1995)
xylazine	50 mg	15 mg (as required)	
Sodium pentobarbital	60 mg	10 mg (as required)	Rovainen et al. (1993)
Sodium pentobarbital plus	25 mg		Hudetz et al. (1992)
ketamine	30 mg		
Urethane	1000 mg	100 mg (as required)	Rovainen et al. (1993)
Urethane plus	600 mg		Ngai et al. (1988)
α-chloralose	50 mg		

[a]Dosing is approximate and will change depending on the emotional state of the animal.

PREPARATION OF ANIMALS

The following protocol was used to prepare the animal for imaging. Unless specified, all pharmaceuticals and surgical supplies were obtained from Henry Schein (Melville, New York). Our experiments were performed on Sprague-Dawley rats, 210–240 g in mass. All procedures were approved by local Institutional Animal Care and Use Committees, following NIH (1985) guidelines. A review of standard preparatory procedures and surgical techniques can be found in van Dongen et al. (1991) and Waynforth and Flecknell (1992).

1. Anesthetize the animal with **urethane**. Deliver the anesthetic intraperitoneally (i.p.) at an initial level of 1.2 g/kg as a split dose over a period of 10 minutes. Supplement at 0.2 g/kg as needed.

   Notes: The depth of anesthesia is sufficient to allow surgical procedures to be carried out when the pedal withdrawal response is lost (Flecknell 1987).

   We prepare a 0.3 g/ml stock solution of urethane, which can be stored at 4°C.

   Urethane is a carcinogen and care must be taken to not breathe the powder.

   Urethane (see Appendix 4 for Caution)

2. Perform the craniotomy above the brain region of interest as follows:

   a. Secure the animal in a stereotaxic holder (e.g., no. 960, David Kopf Instruments; the holder is modified to rotate about the anterior-posterior axis).

   b. Make a succession of glancing cuts along an outline of the craniotomy with a high-speed handpiece (no. 464004, Dentsply Midwest) that is equipped with a 1/2 round bur. Cease to cut just as the bone is observed to craze.

   c. Remove the bone flap with forceps.

d. Protect the surface of the dura from desiccation with a gelatin sponge (Upjohn) soaked in physiological saline or ACSF (see below).

Notes: We consider measurements over primary vibrissa cortex, which is the part of parietal cortex that nominally lies between –1 and –5 mm anterior-posterior to the Bregma point, and between 4 and 7 mm from the midline on the medial-lateral axis (Paxinos and Watson 1986). Somatotopic maps vary between animals (Woolsey et al. 1974), although it appears that their location covaries with that of the cerebral angioarchitecture (Kleinfeld and Delaney 1996). As a practical issue, we found that the center of the primary vibrissa area nominally lies just beneath the origin of the temporalis muscle on the lateral aspect of the temporalis bone and approximately 2 mm caudal to the Bregma point.

We verify the electrophysiological correlate of mechanical stimulation of the vibrissae by an electrocorticogram (see below).

3. To prepare a cranial window, directly glue a metal frame (see Figure 23.1 and note below) to the skull with dental acrylic cement. To achieve a reliable connection between acrylic cement and bone, perform the following:

a. Carefully clean the contact regions on the bone of soft tissue and rub with a cotton applicator.

b. Apply a thin layer of cyanoacrylate cement (Superbonder 49350; Loctite).

c. Rub the skull again to remove excess cyanoacrylate.

Notes: The metal frame, fixed to the skull, surrounds the craniotomy as a means to rigidly hold the head of the animal (Figure 23.1) to the optical apparatus. With the addition of a coverglass window (see step 6, below), this frame also serves to provide a chamber that seals and protects the cortex (Morii et al. 1986; Kleinfeld and Delaney 1996). Resealing the craniotomy is crucial for the suppression of excessive motion that otherwise ensues as a result of cranial-pressure fluctuations that are caused by heartbeat and breathing. With agarose gel between the glass and the cortex (see step 5, below), the cranial opening can be effectively resealed even if a narrow opening is left on the sides as a means to insert glass microelectrodes into cortex (Svoboda et al. 1997).

If an even more stable attachment is desired, #000-3/32 self-tapping screws (Small Parts) can be introduced to the anterior and posterior aspects of the skull. Undersized holes for the screws are drilled with a high-speed handpiece and a 1/4 round bur. The screws, which pass through openings in the frame, are then mechanically linked to the frame with dental acrylic (see Figure 23.1).

4. (*Optional*) To remove the dura, prepare a precision needle by vertically holding a 250–500-μm diameter tungsten wire in a blowtorch flame for several seconds (Hudspeth and Corey 1977). With the needle, gently pick up the dura and pull it away from the brain surface. Then, grasp the dura with two fine forceps (Dumont #5) and tear it into multiple flaps.

Notes: It is possible to image through the intact dura (Kleinfeld et al. 1998). However, to improve imaging conditions and allow electrical mapping of the brain surface, the dura often needs to be removed.

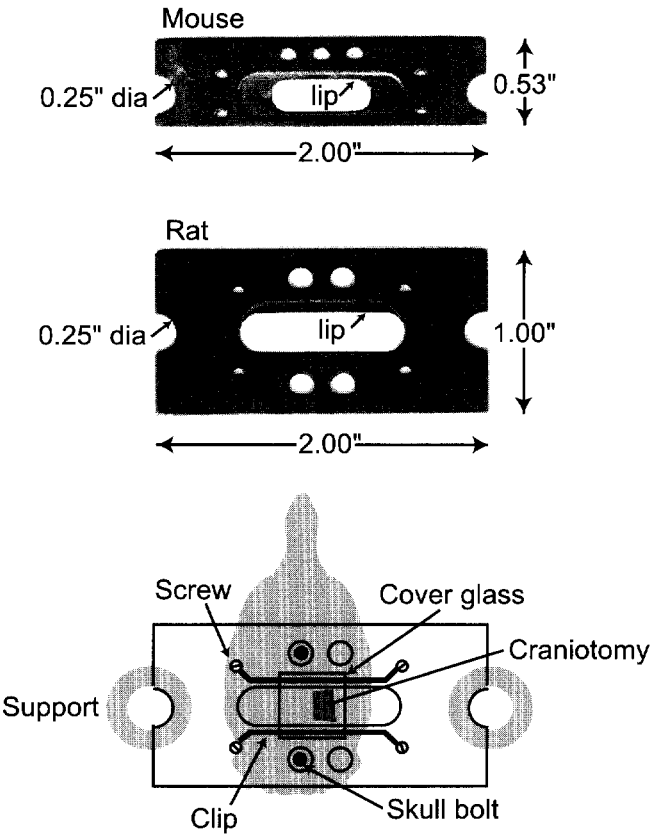

Figure 23.1. Cranial support frames that are used to stabilize the head of a rodent. The frames, as used for mice (*top panel*) or rats (*middle panel*), contain an elongated opening that encompasses the craniotomy (*lower panel*). The frames are constructed of stainless steel ground to a thickness of 0.040 inches. They are attached to the skull either directly with dental acrylic cement, or in conjunction with screws that are placed in the skull so that their heads protrude through openings in the frame (holes b; 0.10 inches in diameter for the mouse frame and 0.15 inches in diameter for the rat frame) which are then encapsulated in cement. The elongated opening (0.20 inches wide for the mouse frame and 0.25 inches wide for the rat frame) contains a lip that is 0.015 inches thick. The lip, together with two beryllium-copper clips that are attached to the frame by number 2-56 slot-head screws (holes a), hold a coverglass in place to form a chamber that is filled with agarose and is sealed along at least two edges; an electrode may be inserted at an oblique angle through the remaining narrow openings (Svoboda et al. 1997). Last, the frame may be attached to standard optical components via the 0.25-inch bolt holes spaced 2.00 inches apart; we use 0.50-inch diameter stainless-steel rods (SP series, Newport) as intermediary supports.

As an alternate method, after an initial tear is made, the dura may be dissected with Vannas scissors. It is crucial to avoid any bleeding, and thus not cut or tear across any large vessel in the dura, because the congealed blood seriously degrades imaging capabilities.

The dura is usually removed after attachment of the metal frame to the rat (see step 3, above). If necessary, the cortical representation of sensory inputs can be

mapped by using a ball electrode to measure evoked surface potentials (Chapin and Lin 1984). The ball electrode is formed by melting the end of a 100 μm to 150 μm diameter silver wire. The reference electrode, and amplification and recording electronics, are the same as that for the electrocorticogram (ECoG) measurements (see below).

5. Fill the chamber with 1–2% LMP agarose.

1–2% Low-melting-point (LMP) agarose

Prepare a 1–2 % (w/v) solution of LMP agarose (no. A-9793, Sigma) in ACSF.

ACSF should contain neither carbonate nor phosphate, which cause precipitation when the solution is boiled to dissolve the agarose.

ACSF

125 mM NaCl
5 mM **KCl**
10 mM glucose
10 mM HEPES
3.1 mM **$CaCl_2$**
1.3 mM **$MgCl_2$**
pH 7.4

Note: Before applying the agarose to the cortical surface, test that the temperature is not above approximately 37°C, by squirting a drop onto the back of the hand.

$CaCl_2$, KCl, $MgCl_2$ (see Appendix 4 for Caution)

6. Seal the chamber using a coverglass (no. 1, cut to size; see note to step 3, above).

Electrocorticogram

A field electrode is placed at the boundary of the primary and secondary vibrissa sensory areas (Carvell and Simons 1986), just lateral to the craniotomy, with a reference in occipital cortex, for ECoG verification of vibrissa stimulation. We use 50-μm Teflon-coated silver wire (no. 7955, AM Systems), with approximately 0.5 mm of the insulation removed at the end, which rests against the cortical surface. Ideally, both the field and reference signals should be electrically buffered close to the animal with a field effect transistor source follower circuit (Horowitz and Hill 1989); a useful solution is to both buffer and amplify the signals with a DAM-80 high input-impedance differential probe (World Precision Instruments).

Maintenance of Body Function

Respiratory Airflow and Body Fluid Volume

Animals receive a prophylactic dose of atropine (0.1 mg subcutaneously [s.c.] every 2 hours) as a prelude against respiratory distress. Body fluids are supplemented through an s.c. injection of physiological saline (0.9% [w/v] NaCl) supplemented with 5% (w/v) dextrose (10 ml/kg/hr).

Temperature

Body temperature is maintained near 37°C using a heating blanket (no. 507053, Harvard Apparatus). Note that the temperature probe that comes with most systems is encased in a sheath that is too large for use with mice or rat pups; this sheath may be removed and the actual probe coated with silicone elastomer (Sylgard 184, Dow Corning) or nail polish (Wet 'n' Wild, Pavion) for use with small rodents. In all cases, the probe is coated with petroleum jelly prior to insertion, and the associated cable is taped to a hindlimb.

Eyes

The eyes are protected against dessication by drops of mineral oil.

Heart Rate and Respiratory Rate

Measurements of the heart rate and respiratory rate provide a crucial set of indicators to monitor the health of the animal and can also be used to correctly interpret periodic components in the blood-flow signal. In healthy anesthetized rats, the heart rate is between 5 and 7 Hz and the respiration rate is between 1.5 and 2 Hz.

The EKG is measured by placing needle electrodes diagonally across a pair of front and hind limbs, buffering the resultant electrical signal with a high-impedance amplifier, and bandpass filtering; the DAM40 (World Precision Instruments) is an example of a low-cost amplifier/filter suitable for this measurement. The respiratory rate is measured by placing a small thermocouple just outside a nostril of the animal to detect the periodic temperature fluctuations caused by the breathing-dependent variation in airflow. We recommend using a pair of 36-gauge fine-wire thermocouples (5TC series, Omega Engineering) connected back-to-back for a differential measurement against a room-temperature reference and amplified with a differential input amplifier, such as the DAM40 (World Precision Instruments). (With the thermocouple leads denoted A/B for the respiratory signal pair and a/b for the reference pair, and the amplifier inputs labeled +/–, the order of connections is +/A/B/b/a/–.)

Blood Pressure

Many researchers find it desirable to measure the blood pressure via a catheter that is inserted into the femoral artery; the BLPR transducer and BP-1 monitor (World Precision Instruments) comprise a particular low-cost solution for this purpose. In experiments in which the issue of exchange gas is central, a tracheotomy is performed and the tidal CO_2 is measured; surplus neonatal monitors provide an economical source of equipment. Animals can also be paralyzed (1 mg/kg/hr D-tubocurarine chloride) and ventilated (no. 55-3538, Harvard Apparatus) for complete control of respiration and blood gases.

Dye Labeling

Blood Serum

Blood serum is labeled most simply through a tail-vein injection, although some researchers inject the dye through the femoral artery. The tail veins lie just lateral to the midline. The following protocol is used for labeling blood serum of rats.

1. Submerge the tail in 37°C H_2O for approximately 2 minutes to make the veins dilate.
2. Starting as close to the tip of the tail as possible, to permit multiple penetrations, insert a 24-gauge catheter and inject a 0.5-ml bolus of dye.

   Notes: This volume is to be compared with the approximately 21 ml total blood volume (~10 ml serum volume) for a 250 g rat (Farrell 1991).

   We used 5% (w/v) solution of FITC dextran (10 kD; FD-10S, Sigma) to label the blood serum in our initial study (Kleinfeld et al. 1998). In general, different investigators report the successful use of FITC-labeled dextran and rhodamine–dextran with molecular masses up to 150,000 kD. Although the serum may be labeled with the sodium salt of dyes, we found that Na-fluorescein is appreciably absorbed by the surrounding tissue.
3. Repeat dye injections at intervals of 2–3 hours. We record for as long as 6 hours.

Red Blood Cells

FITC may be used to label the RBCs from a donor animal, which may be transfused into a second animal (Sarelius and Duling 1982). This allows the motion of RBCs to be measured as bright objects on a dark background, as opposed to measuring RBCs as dark objects against a bright background for the case of labeled serum. RBC labeling of a fraction of the available pool is advantageous when measuring flow at high RBC density, as a means to better discriminate individual cells (Hudetz 1997).

MEASUREMENTS

We imaged the fluorescent serum and acquired data with a laser scanner and upright microscope system described in Svoboda et al. (1997 and Chapter 22). Our objective was a 40x water-immersion lens (Zeiss). The total average power delivered to the cortex ranged from 30 mW to 300 mW; higher values were required to image at greater depths in the brain to compensate for the scattering of incident light. The total average power delivered to the focus was less than 10 mW.

Planar Scans

A single, planar image appears to contain fragments of individual blood vessels (Figure 23.2a). The intensity distribution from a series of such images, acquired at successive depths through the cortex, can be used to infer the attenuation of the detected fluorescent light as a function of depth below the pia (Figure 23.2b). The distribution of intensity values is dominated by a large peak, presumed to be largely fluorescence from dye that permeated the tissue, as well as some autofluorescence, and a tail at higher intensities due to the dye in the blood serum. Both features of the spectrum shift toward lower intensity values as the focus moves deeper into the brain.

We can estimate a penetration constant based on the assumption that the fluorescent yield of the label is independent of depth. The average value of the intensity in the brightest 1000 pixels of the tail decreases as a function of depth, as shown in Figure 23.2c (note that the power was reset near depths of 175 and 375 μm). The decrease in measured intensity for this experiment is roughly exponential with an attenuation length that lies between 80 μm (fit to depths > 200 μm; insert, Figure 23.2c) and 100 μm (fit to all depths; insert, Figure 23.2c). The peak of the distribution, which is a measure of the background intensity, is well described by an exponential decay (Figure 23.2d) with an attenuation length of approximately 100 μm (insert, Figure 23.2d). If we assume a detection efficiency that is largely independent of the depth, the falloff constant for the excitation intensities is then roughly 200 μm because of the quadratic intensity dependence of two-photon excitation on the incident power.

The complete angioarchitecture of a column of the cortex, approximately 200 x 200 x 600 μm with the 40x objective, can be reconstructed from a set of planar scans that are corrected for the attenuation with increasing depth and, if applicable, changes in incident laser power (Kleinfeld et al. 1998). Furthermore, the above analysis of the decrease in average intensity of the labeled vessels as a function of depth below the pia could, in the future, be used to compare the optical penetration of excitation light of different wavelengths.

Blood Flow and Line Scans

We readily imaged single microvessels (Figure 23.3a) whose caliber was determined from the measured cross section in a planar image (side panel, Figure 23.3a). Successive,

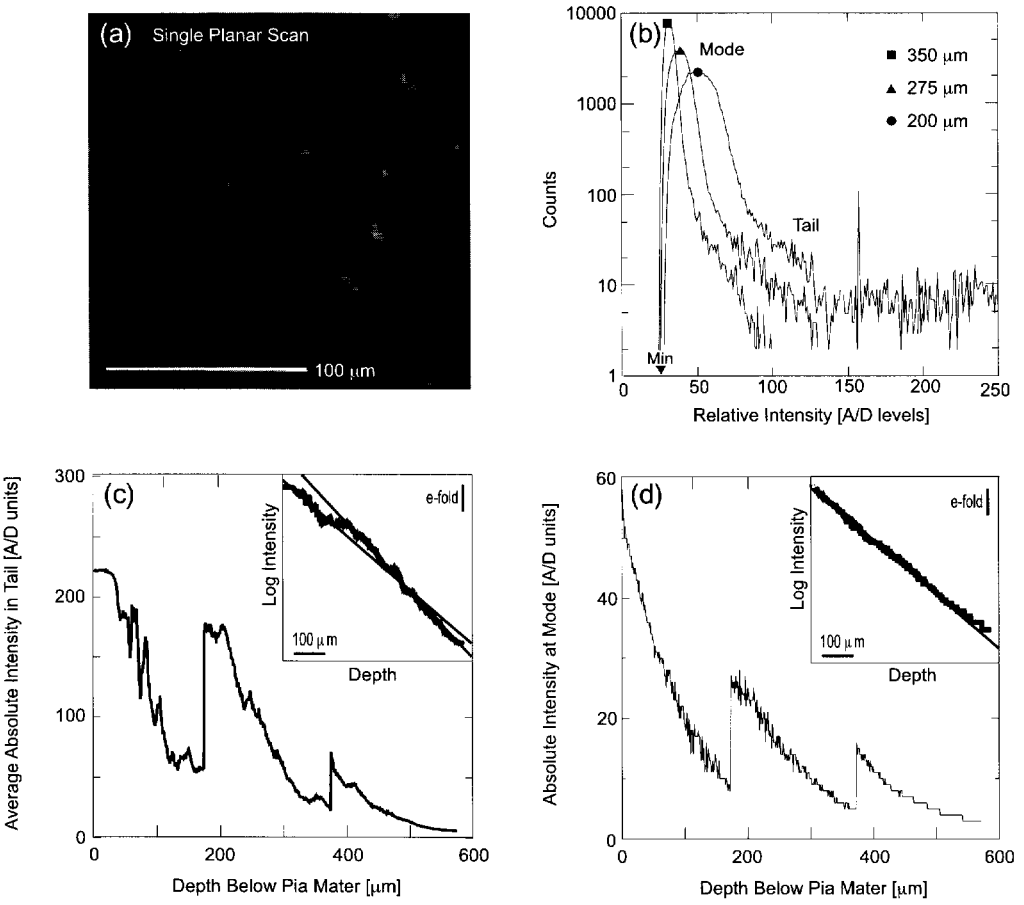

Figure 23.2. Planar scans and the attenuation of the two-photon-induced fluorescence signal. (*a*) A 170 x 170 μm single planar scan at a depth of 275 μm below the pia mater. The dark stripes in vessels correspond to the location of unlabeled RBCs at the time of the scan. (*b*) The distribution of intensities from three scans at three different depths. The low-intensity edge at 26 A/D (analog/digital) units, labeled "Min," corresponds to the dark level. (*c*) The average absolute intensity in the tail of the distributions, computed as an average over the brightest 1000 pixels with the dark level subtracted off, as a function of depth. We confirmed, by examining the integral of each distribution, that each planar scan contained at least 1000 pixels in the tail. Note that the two jumps in the intensity correspond to a manual increase in power and that the initial flat portion of the distribution results from saturated pixels. The insert shows the logarithm of the intensity, with all three segments joined together. The two straight lines correspond to fits to the data: The shallower line through the entire data set corresponds to an exponential decay with an attenuation length of 100 μm and the steeper line that fits the middle and lower part of the curve has an attenuation length of 80 μm. (*d*) The intensity at the mode of the distributions as a function of depth. The insert shows the logarithm of the intensity; the straight line is a fit with an attenuation length of 100 μm.

rapidly acquired planar images of such microvessels revealed a succession of dark objects that moved across a sea of fluorescently labeled serum (Figure 23.3b). The dark spots are RBCs, which exclude the dye and are therefore not fluorescent (Dirnagl et al. 1992). The change in position of the spots between successive images is proportional to the veloci-

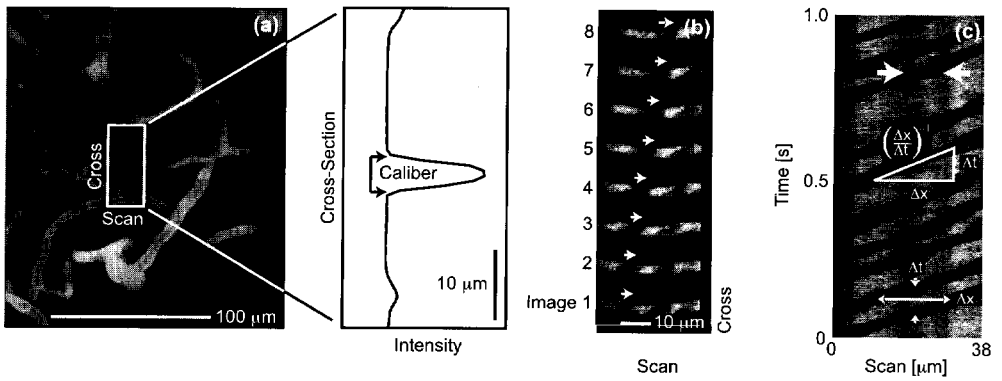

Figure 23.3. Parameterization of blood flow in a capillary. (*a*) Horizontal view in the vicinity of a capillary. The image is the maximal projection from a contiguous set of 100 planar scans acquired every 1 μm between 310 and 410 μm. The side panel shows the intensity profile along the cross section for the scan that passed through the central axis of the capillary in question. The caliber is estimated from the number of pixels whose intensity is above the background level, as noted. (*b*) Successive planar images, acquired every 16 msec, through a capillary at a depth of 450 μm. The change in position of a particular unstained object, interpreted as an RBC, is indicated by the series of arrows; the velocity of the RBC is +0.11 mm/sec. (*c*) Line scan through a capillary at a depth of 600 μm. In this imaging modality, the RBCs appear as dark bands. The annotations illustrate how RBC flow can be parameterized as a function of space and time. The instantaneous flux is $1/\Delta t$, the linear density is $1/\Delta x$, and the velocity is $\Delta x/\Delta t$, as indicated. The width of the dark band (*heavy arrows*) is a measure of the profile of the RBC along the scan direction.

ty (arrows, Figure 23.3b). Although in this particular case the speed of the RBCs was sufficiently low to allow us to capture their motion by comparing the positions of dark spots in successive frames, this is not the case in general. To achieve higher time resolution, we acquired repetitive scans along the central axis of a capillary (Dirnagl et al. 1992), i.e., line-scans, to characterize the flow of RBCs in capillaries.

The data in line-scan mode comprise a matrix with one spatial and one temporal dimension. The motion of RBCs leads to dark bands in the data set (Figure 23.3c). The average time between bands at a fixed position, denoted Δt, is inversely proportional to the flux, the average distance between bands at a fixed time, denoted Δx, is inversely proportional to the density of RBCs, and the slope of the band, $\Delta t/\Delta x$, is inversely proportional to the velocity of the RBCs (insert, Figure 23.3c). These three quantities are related by **flux = density x velocity.** The flux and velocity were directly extracted from the data (Kleinfeld et al. 1998) and allow the parameterization of the blood flow.

A particularly interesting example of line-scan data involved the determination of blood flow at a junction of three vessels. We observed many such junctions in which two of the three arms were collinear, which allowed us to simultaneously monitor flow in the two collinear arms. The flow was observed to be highly irregular at such junctions and often exhibited reversals in direction, as shown in epochs from successive trials with the same vessel (Figure 23.4). These data suggest that capillary flow is shunted in loops, consistent with the plexuses of microvessels (Motti et al. 1986) and sphincters (Nakai et al. 1981) in neocortex.

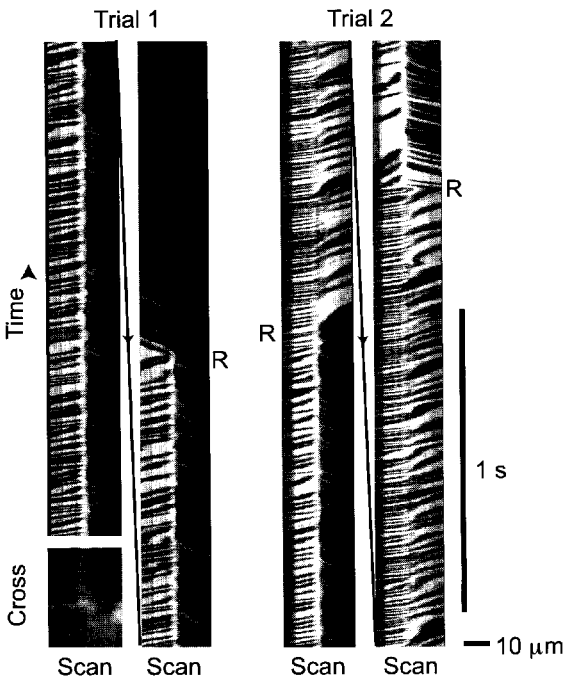

Figure 23.4. Examples of reversals in the direction of flow observed by simultaneously monitoring RBC motion in two collinear arms of a T-junction at a depth of 260 μm. The lower left panel is a planar scan of the junction. The two data sets, labeled trials 1 and 2, correspond to approximately 4-second intervals of line-scan measurements (cut and offset for display purposes) that were performed 5 min apart. Note the reversal, labeled "R," in the direction of flow in the arm on the left in the first trial shown and the sequence of reversals in the right arm in the second trial.

CONCLUSIONS AND FUTURE DIRECTIONS

We have shown that two-photon laser scanning microscopy can be used to image the flow of RBCs at least 600 μm below the pial surface in rat. This range encompasses layer 2/3 of neocortex as well as the superficial part of layer 4, the level of the dominant thalamic input to neocortex. The further optimization of laser parameters may allow two-photon microscopy to be used to probe blood flow at even greater depths without a loss in resolution. However, significant increases in peak laser powers may induce large background signals, and possibly photodamage, through the absorption of out-of-focus laser light in the upper layers of cortex.

We anticipate that two-photon microscopy will provide a novel tool to study the microscopic coupling of blood flow to neuronal activity. It is likely that future studies will be of greatest value when blood-flow measurements are performed simultaneously with measurements of neighboring neuronal or glial activity, either in conjunction with microelectrode recordings or with functional indicators of activity. Furthermore, although we focused solely on the motion of RBCs, the motions of the serum and of leukocytes are also amenable to experimental observation.

REFERENCES

Armstrong-James M., Fox K., and Das-Gupta A. 1992. Flow of excitability within barrel cortex on striking a single vibrissa. *J. Neurophysiol.* **68:** 1345–1358.

Blasdel G.G. and Salama G. 1986. Voltage-sensitive dyes reveal a modular organization in monkey striate cortex. *Nature* **321:** 579–585.

Carvell G.E. and Simons D.J. 1986. Somatotopic organization of the second somatosensory area (SII) in the cerebral cortex of the mouse. *Somatosens. Res.* **3:** 213–237.

Chapin J.K. and Lin C.-S. 1984. Mapping the body representation in the SI cortex of anesthetized and awake rats. *J. Comp. Neurol.* **229:** 199–213.

Chapin J.K., Waterhouse B.D., and Woodward D.J. 1981. Differences in cutaneous sensory response properties of single somatosensory cortical neurons in awake and halothane anesthetized rats. *Brain Res. Bull.* **6:** 63–70.

Denk W., Piston D.W., and Webb W. 1995. Two-photon molecular excitation in laser-scanning microscopy. In *Handbook of biological confocal microscopy,* 2nd edition (ed. J.W. Pawley), pp. 445–458. Plenum Press, New York.

Denk W., Strickler J.H., and Webb W.W. 1990. Two-photon laser scanning fluorescence microscopy. *Science* **248:** 73–76.

Denk W., Delaney K.R., Kleinfeld D., Strowbridge B., Tank D.W., and Yuste R. 1994. Anatomical and functional imaging of neurons and circuits using two photon laser scanning microscopy. *J. Neurosci. Methods* **54:** 151–162.

Dirnagl U., Villringer A., and Einhaupl K.M. 1992. *In-vivo* confocal scanning laser microscopy of the cerebral microcirculation. *J. Microsc.* **165:** 147–157.

Farrell A.P. 1991. Circulation of body fluids. In *Environmental and metabolic animal physiology* (ed. C.L. Prosser), pp. 509–558. Wiley-Liss, New York.

Flecknell P.A. 1987. *Laboratory animal anesthesia: An introduction for research workers and technicians.* Academic Press, San Diego.

Golanov E.V., Yamamoto S., and Reis D.J. 1994. Spontaneous waves of cerebral blood flow associated with a pattern of electrocortical activity. *Am. J. Physiol.* **266:** R204–R214.

Grinvald A., Lieke E.E., Frostig R.D., Gilbert C.D., and Wiesel T.N. 1986. Functional architecture of cortex revealed by optical imaging of intrinsic signals. *Nature* **324:** 361–364.

Horowitz P. and Hill W. 1989. *The art of electronics.* Cambridge University Press, Cambridge, United Kingdom.

Hudetz A.G. 1997. Blood flow in the cerebral capillary network: A review emphasizing observations with intravital microscopy. *Microcirculation* **4:** 233–252.

Hudetz A.G., Weigle C.G.M., Fendy F.J., and Roman R.J. 1992. Use of fluorescently labeled erythrocytes and digital cross-correlation for the measurement of flow velocity in the cerebral microcirculation. *Microvasc. Res.* **43:** 334–341.

Hudspeth A.J. and Corey D.P. 1977. Sensitivity, polarity, and conductance change in the response of vertebrate hair cells to controlled mechanical stimuli. *Proc. Natl. Acad. Sci.* **74:** 2407–2411.

Johns C., Gavras I., Handy D.E., Salomao A., and Gavras H. 1996. Models of experimental hypertension in mice. *Hypertension* **28:** 1064–1069.

Kleinfeld D. and Delaney K.R. 1996. Distributed representation of vibrissa movement in the upper layers of somatosensory cortex revealed with voltage sensitve dyes (erratum 1997, **378:** 594). *J. Comp. Neurol.* **375:** 89–108.

Kleinfeld D., Mitra P.P., Helmchen F., and Denk W. 1998. Fluctuations and stimulus-induced changes in blood flow observed in individual capillaries in layers 2 through 4 of rat neocortex. *Proc. Natl. Acad. Sci.* **95:** 15741–15746.

Lindauer U., Villringer A., and Dirnagl U. 1993. Characterization of CBF response to somatosensory stimulation: Model and influence of anesthetics. *Am. J. Physiol.* **264:** H1223–H1228.

Merrill D.C., Granwehr B.P., Davis D.R., and Sigmond C.D. 1997. Use of transgenic and gene-targeted mice to model the genetic basis of hypertensive disorders. *Proc. Assoc. Am. Physicians* **109:** 533–546.

Morii S., Ngai A.C., and Winn H.R. 1986. Reactivity of rat pial arterioles and venules to adenosine and carbon dioxide: With detailed description of the closed cranial window technique in rats. *J. Cereb. Blood Flow Metab.* **6:** 34–41.

Motti E.D., Imhof H.-G., and Yasargil M.G. 1986. The terminal vascular bed in the superficial cortex of the rat: An SEM study of corrosion casts. *J. Neurosurg.* **65:** 834–846.

Muldoon S.M., Hart J.L., Bowen K.A., and Freas W. 1988. Attenuation of endothelium-mediated vasodilation by halothane. *Anesthesiology* **68:** 31–37.

Nakai K., Imai H., Kamei I., Itakura T., Komari N., Kimura H., Nagai T., and Maeda T. 1981. Microangioarchitecture of rat parietal cortex with special reference to vascular "sphincters": Scanning electron microscopic and dark field microscopic study. *Stroke* **12:** 653–659.

National Institutes of Health (NIH). 1985. *Guide for the care and use of laboratory animals* (NIH Publ. 85-23). National Institutes of Health, Bethesda, Maryland.

Ngai A.C., Ko K.R., Morii S., and Winn H.R. 1988. Effect of sciatic nerve stimulation on pial arterioles in rats. *Am. J. Physiol.* **254:** H133–H139.

Ogawa S., Lee T.-M., Nayak A.S., and Glynn P. 1990. Oxygenation-sensitive contrast in magnetic resonance image of rodent brain at high fields. *Magn. Reson. Med.* **14:** 68–78.

Paxinos G. and Watson C. 1986. *The rat brain in stereotaxic coordinates.* Academic Press, San Diego.

Rovainen C.M., Woolsey T.A., Blocher N.C., Wang D.-B., and Robinson O.F. 1993. Blood flow in single surface arterioles and venules on the mouse somatosensory cortex measured with videomicroscopy, fluorescent dextrans, nonoccluding fluorescent beads, and computer-assisted image analysis. *J. Cereb. Blood Flow Metab.* **13:** 359–371.

Sarelius I.H. and Duling B.R. 1982. Direct measurement of microvessel hematocrit, red cell flux, velocity, and transit time. *Am. J. Physiol.* **243:** H1018–H1022.

Short C.E. 1987. *Principles and practice of veterinary anesthesia.* Williams and Wilkins, Baltimore, Maryland.

Svoboda K., Denk W., Kleinfeld D., and Tank D.W. 1997. In vivo dendritic calcium dynamics in neocortical pyramidal neurons. *Nature* **385:** 161–165.

van Dongen J.J., Remie R., Remsema J.W., and van Wunnik G.H.J. 1991. *Manual of microsurgery of the laboratory rat.* Elsevier, New York.

Villringer A., Haberl R.L., Dirnagl U., Anneser F., Verst M., and Einhaupl K.M. 1989. Confocal laser microscopy to study microcirculation on the rat brain surface in vivo. *Brain Res.* **504:** 159–160.

Waynforth H.B. and Flecknell P.A. 1992. *Experimental and surgical techniques in the rat.* Academic Press, San Diego.

Wei L., Rovainen C.M., and Woolsey T.A. 1995. Ministrokes in rat barrel cortex. *Stroke* **26:** 1459–1462.

West M.O. 1998. Anesthetics eliminate somatosensory-evoked discharges of neurons in the somatotopically organized sensorimotor striatum of the rat. *J. Neurosci.* **18:** 9055–9068.

Woolsey T.A. and Van Der Loos H. 1970. The structural organization of layer IV in the somatosensory region (SI) of mouse cerebral cortex. *Brain Res.* **17:** 205–242.

Woolsey T.A., Welker C., and Schwartz R.H. 1974. Comparative anatomical studies of the SmI

face cortex with special reference to the occurrence of "barrels" in layer IV. *J. Comp. Neurol.* **164:** 79–94.

Woolsey T.A., Rovainen C.M., Cox S.B., Henger M.H., Liange G.E., Liu D., Moskalenko Y.E., Sui J., and Wei L. 1996. Neuronal units linked to microvascular modules in cerebral cortex: Response elements for imaging the brain. *Cereb. Cortex* **6:** 647–660.